

Superconducting properties of $K_{1-x}Na_xFe_2As_2$ under pressure

V. Grinenko,* W. Schottenhamel, A.U.B. Wolter, D.V. Efremov,
S.-L. Drechsler, S. Aswartham†, M. Kumar, and S. Wurmehl

Leibniz-Institute for Solid State and Materials Research, IFW-Dresden, D-01171 Dresden, Germany

M. Roslova and I. V. Morozov

*Leibniz-Institute for Solid State and Materials Research, IFW-Dresden, D-01171 Dresden, Germany and
Lomonosov Moscow State University, GSP-1, Leninskie Gory, Moscow, 119991, Russian Federation*

B. Holzapfel

*Leibniz-Institute for Solid State and Materials Research, IFW-Dresden, D-01171 Dresden, Germany and
Karlsruhe Institute of Technology (KIT), Hermann-von-Helmholtz-Platz 1, 76344 Eggenstein-Leopoldshafen, Germany*

B. Büchner

*Leibniz-Institute for Solid State and Materials Research, IFW-Dresden, D-01171 Dresden, Germany and
Institut für Festkörperphysik, TU Dresden, D-01062 Dresden, Germany*

E. Ahrens

Institut für Anorganische Chemie, TU Dresden, D-01062 Dresden, Germany

S. I. Troyanov

Lomonosov Moscow State University, GSP-1, Leninskie Gory, Moscow, 119991, Russian Federation

S. Köhler, E. Gati, S. Knöner, N. H. Hoang, and M. Lang
Goethe University, Max-von-Laue-Strasse 1, 60438, Frankfurt am Main

F. Ricci‡ and G. Profeta

*CNR-SPIN and Dipartimento di Scienze Fisiche e Chimiche,
Università degli Studi dell'Aquila, Via Vetoio 10, I-67100 L'Aquila, Italy
(Dated: June 19, 2021)*

The effect of hydrostatic pressure and partial Na substitution on the normal-state properties and the superconducting transition temperature (T_c) of $K_{1-x}Na_xFe_2As_2$ single crystals were investigated. It was found that a partial Na substitution leads to a deviation from the standard T^2 Fermi-liquid behavior in the temperature dependence of the normal-state resistivity. It was demonstrated that non-Fermi liquid like behavior of the resistivity for $K_{1-x}Na_xFe_2As_2$ and some KFe_2As_2 samples can be explained by disorder effect in the multiband system with rather different quasiparticle effective masses. Concerning the superconducting state our data support the presence of a shallow minimum around 2 GPa in the pressure dependence of T_c for stoichiometric KFe_2As_2 . The analysis of T_c in the $K_{1-x}Na_xFe_2As_2$ at pressures below 1.5 GPa showed, that the reduction of T_c with Na substitution follows the Abrikosov-Gor'kov law with the critical temperature T_{c0} of the clean system (without pair-breaking) which linearly depends on the pressure. Our observations, also, suggest that T_c of $K_{1-x}Na_xFe_2As_2$ is nearly independent of the lattice compression produced by the Na substitution. Further, we theoretically analyzed the behavior of the band structure under pressure within the generalized gradient approximation (GGA). A qualitative agreement between the calculated and the recently in de Haas-van Alphen experiments¹ measured pressure dependencies of the Fermi-surface cross-sections has been found. These calculations, also, indicate that the observed minimum around 2 GPa in the pressure dependence of T_c may occur without a change of the pairing symmetry.

PACS numbers: 74.25.Bt, 74.25.Dw, 74.25.Jb, 65.40.Ba

I. INTRODUCTION

Recently, KFe_2As_2 (K-122) has attracted special attention due to several unusual physical properties such as a very large quasiparticle effective mass^{1,3-6} and superconductivity (SC) with nodes in the superconducting gap⁴⁻⁹. Such a large mass enhancement is usually ascribed to the

†Dept of Physics and Astronomy, University of Kentucky, Lexington, USA

presence of pronounced correlation effects.¹⁰ However, in the present case the nature and the strength of these correlation effects as well as the symmetry of the superconducting order parameter are still under debate. Some experiments were interpreted in favor of s_{\pm} -wave SC with accidental nodes^{9,11–13} whereas other favor d - wave SC^{5,7,8,14,15}. Based on their theoretical calculations the authors of Ref. 16 argue that the electronic correlations are enhanced in the strongly hole-overdoped K-122 as compared to lower hole doping levels in other 122 systems due to the changes in the Fermi-surface topology. This might affect the low-energy spin excitation spectra and cause an increasing density of states (DOS) at the Fermi energy E_F . However, this calculation underestimates the correlation effect found experimentally. Recently, it was proposed that the unexpected large effective mass enhancement of the order of 9 to 10 could be related to the proximity of an orbital-selective Mott transition for K-122⁴. The relation between the enhanced correlation effects and the SC remains still unclear. Therefore, tuning of the physical properties of K-122 by external or chemical pressure and disorder can provide more insight into the pairing symmetry and the present correlation effects.

Recently, several studies of the physical properties of K-122^{1,2,17–21} and its sister compounds Cs-122^{21–23}, and Rb-122^{24–27} under external pressure have been reported. F.F. Tafti *et al.* observed that the superconducting critical temperature T_c of K-122 at first monotonically decreases with increasing hydrostatic pressure, then reaches a minimum at $P \sim 1.7$ GPa (we adopt from Ref. 2 referring $P = 1.7$ GPa as critical pressure), and finally shows a reversal behavior^{2,21}. The value of the critical pressure is nearly independent of the amount of the disorder in K-122 but it is reduced in the unsubstituted clean Cs-122²¹. However, V. Taufour *et al.*, showed that the pressure dependence of T_c for K-122 is sensitive to the pressure medium¹⁹, and that for the best pressure (hydrostatic) conditions the reversal behavior of T_c is replaced by a broad minimum followed by a nearly pressure independent T_c value above 2.5 GPa. From the almost pressure independent behavior of the Hall coefficient extrapolated to $T = 0$ as well as from the residual resistivity, it was concluded that the topology of the Fermi surface does not change across the critical pressure.^{2,28} This point of view was, also, supported by recent de Haas-van Alphen (dHvA) measurements under pressure, where at least two small but accessible Fermi surface sheets (FSS), namely the smallest cylinder α around the Γ -point and the propeller blade-like FSS ϵ around the X point of the Brillouin zone (BZ), do not show a Lifshitz transition up to 2.47 GPa.¹ The evolution of the Fermi surface is accompanied by a reduction of the effective quasi-particle masses without any special feature at the critical pressure. The reduction of the effective masses and the decrease of T_c up to the pressure about 2 GPa can be qualitatively explained by a reduction of coupling constants. In order to explain the T_c minimum it was supposed that

at the critical pressure a change of the superconducting gap symmetry from d - wave to s_{\pm} - wave^{2,21} or from nodal s_{\pm} -wave to a nodeless one¹ should occur. The fast increase of the inelastic scattering rate at the critical pressure obtained from the transport measurements supports such a hypothesis.²¹ Alternatively, V. Taufour *et al.* proposed that a change of symmetry under pressure may not occur at all.¹⁹ These authors empirically supposed that the critical pressure could be a consequence of anisotropic pressure derivatives, since the pressure derivatives along the a axis and the c axis are negative and positive, respectively. In this case, the critical pressure corresponds to the critical pressure in the ab plane above which the slope of $T_c(P)$ depends on the value of $\partial T_c / \partial P_c > 0$, only, whereas $\partial T_c / \partial P_{ab} \equiv 0$ for $P \geq 2$ GPa. These authors have also shown quantitatively that the behavior of the upper critical fields in crossing the critical pressure can be accounted for by k_z modulations of the superconducting gap, only.

The amount and type of disorder provide additional possibilities to tune the superconducting properties. Recently, the effect of Na substitution on the superconducting and the normal-state properties of K-122 was investigated.^{5,7} It was shown that the temperature dependence of the specific heat of $K_{1-x}Na_xFe_2As_2$ single crystals can be explained by multiband d -wave SC. The disorder induced by the Na substitution suppresses the small superconducting gaps and leads to gapless SC with a large residual DOS. The specific heat jump scales approximately with a power-law, $\Delta C_{el} \propto T_c^\beta$, with $\beta \approx 2$ determined by the impurity scattering rate, in contrast to most iron-pnictide superconductors described by the remarkable Bud'ko-Ni-Canfield (BNC) scaling $\Delta C_{el} \propto T^3$.^{18,29} However, the Na substitution might also produce chemical pressure which could additionally affect T_c .

In this work, we show that a partial Na substitution produces non-hydrostatic chemical pressure with a larger compression along the c axis. Thereby the netto (total) effect of the chemical pressure on T_c is strongly reduced due to anisotropic pressure derivatives with different signs along the c and $a(b)$ axis. Therefore, the pressure dependence of T_{c0} (without pair-breaking) and the corresponding coupling constant are nearly independent of the Na substitution. Furthermore, we present a theoretical analysis of the band structure of KFe_2As_2 under pressure within the first-principles density functional theory in the generalized gradient approximation (GGA). The calculations indicate that the minimum in the pressure dependence of T_c can be qualitatively explained by a relatively small non-monotonic variation of the density of states (DOS) at the Fermi level. In general, our results suggests that the superconductivity in K-122 is driven by a single leading band.

II. EXPERIMENTAL

$K_{1-x}Na_xFe_2As_2$ single crystals with a typical mass of about 1-2 mg and several mm in-plane dimensions were grown by the self-flux method. The compositions and the phase purity of the investigated samples were determined by an EDX analysis in a scanning electron microscope, and by x-ray analysis; for details see Refs. 5,7. The two stoichiometric KFe_2As_2 samples were prepared using different fluxes: S1 from a FeAs flux and S2 from a KAs one, for details see Refs.^{30,31}. Additionally, we performed single crystal diffraction measurements at room temperature and at $T = 100$ K. The crystallographic parameters were extracted from single crystal diffraction data. The room temperature single crystal X-ray diffraction data were collected on a Bruker Kappa APEX-II CCD diffractometer using Mo- $K\alpha$ radiation. ϕ - and ω -scans were recorded with an increment of 0.3, integration and corrections for oblique incidence and polarization were performed within SAINT³². A multi-scan absorption correction was applied using SADABS³³. Structure solutions and refinements were done with the JANA2006 package³⁴. Single crystal X-ray diffraction analysis at $T = 100$ K was carried out with an IPDS (STOE) diffractometer using graphite monochromated Mo- $K\alpha$ radiation. Numerical absorption corrections were applied for both data sets with transmission coefficients of $T_{min}/T_{max} = 0.0077/0.3052$ and $0.0495/0.06333$, respectively. The structures were solved and anisotropically refined with the SHELX program package.³⁵ The relative Na/K contents were included into the refinements as an independent parameter (x).

The temperature dependence of the electrical resistivity was measured by the standard four-contact method in the Quantum Design Physical Property Measurement System (PPMS). The temperature dependent, zero-field-cooled (ZFC) magnetization under pressure was measured in a Quantum Design MPMS-SQUID magnetometer down to 1.8 K in a magnetic field of 10 Oe. The samples position was not perfectly fixed during the magnetization measurements under pressure. Therefore, in some cases samples could be tilted with respect to the applied field direction after the application of the pressure. This affects the amplitude of the superconducting diamagnetic signal (due to a variation in the demagnetization factor) as can be seen in Fig. 2. However, the defined T_c values are not affected considerably, since the measurements were performed at low applied magnetic field as compared to the critical fields of the investigated samples.

For the DC magnetization measurement under pressure, we used a commercial pressure cell easyLab Mcell 10 tailored for a MPMS of Quantum Design for the pressure measurements up to 1 GPa and a homemade pressure cell (HPC) for the pressure measurements up to 3 GPa. The HPC has been constructed for a commercial MPMS. Its cell design is mostly related to a diamond anvil cell (DAC), in which two opposing cone-shaped ce-

ramic anvils compress a gasket that serves as the sample chamber.³⁶⁻³⁸ A supplied uniaxial pressure will be transformed into uniform hydrostatic pressure by using Daphne7373 oil as transmitting medium. The cell can be equipped with different types of sample chambers, for which the sample space varied between either 0.7 mm in diameter and 0.4 mm in depth, or on the other hand 0.3 mm in diameter and 0.2 mm in depth. Using these different chambers a maximum hydrostatic pressure up to 3 GPa and 6 GPa can be generated, respectively. Each mechanical part of the pressure cell, except for the anvils, is made from a very low-magnetic CuBe alloy, which allows measurements at a weak background signal of the cell itself.³⁹ Additionally, the magnetization data have been corrected for the contribution of the background signal by subtracting the extrapolated (below T_c) background signal obtained at $T > T_c$. The pressure was determined at low temperatures using superconducting Sn in case of the Quantum Design pressure cell and Pb in case of the homemade cell as a low-temperature pressure gauge.

For most of the measurements the pressure dependence of T_c was linear up to 1.5 GPa (see Fig. 3). However, using the easyLab Mcell 10 pressure cell in some cases we observed deviations from a linear $T_c(P)$ dependence at pressures below 0.1 GPa. To verify the origin of this behavior at low pressures, we performed additional measurements in a He-gas CuBe pressure cell up to the maximum pressure of 0.5 GPa. In the experiment a CuBe cell connected to a He-gas compressor was used for finite P measurements.⁴⁰ An In sample was used for an in-situ determination of the pressure.⁴¹ The use of 4-He as a pressure-transmitting medium ensures truly hydrostatic pressure conditions at low temperatures.^{19,42} The susceptibility data have been corrected for the contribution of the sample holder, including the pressure cell, which was determined independently. In the case of the experiments with He as a pressure medium the non-linear behavior in the $T_c(P)$ dependence at low pressures was not observed. Therefore, we may conclude that the observed deviation from the linear $T_c(P)$ dependence is related to deviation from the hydrostatic conditions. In this work, we consider the data with a linear $T_c(P)$ dependence at low pressure, only, assuming that in this case the measurements were performed under hydrostatic pressure conditions.

III. RESULTS

A. Resistivity and Magnetization

Fig.1 shows the T dependence of the electrical resistivity $\rho(T)$ of $K_{1-x}Na_xFe_2As_2$ single crystals. To remove the uncertainty in the absolute value of $\rho(T)$ between our transport data and the published one in literature associated with geometric factors, we used a normalization

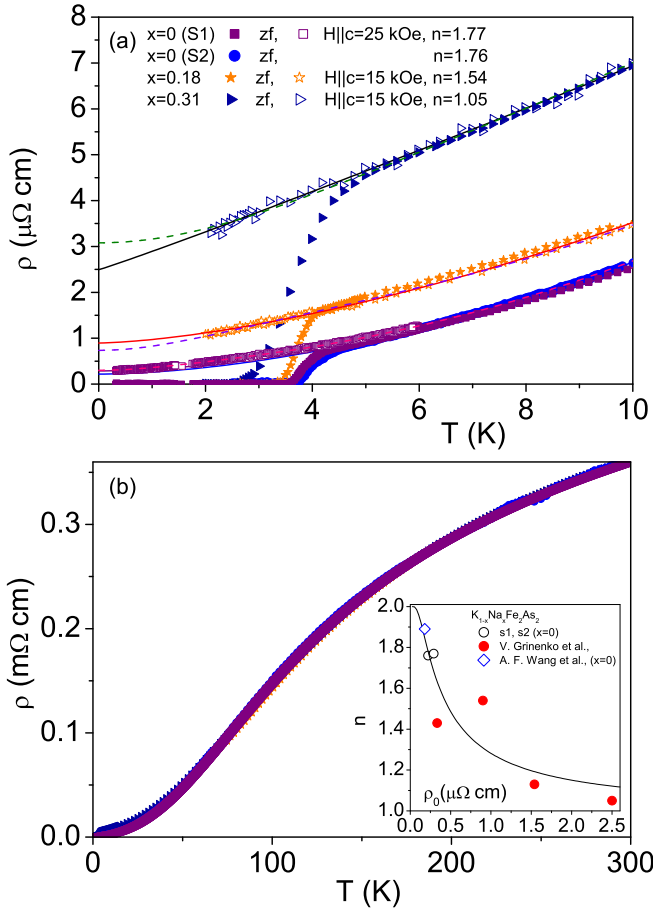


FIG. 1: (color online) The T dependence of the resistivity of $K_{1-x}Na_xFe_2As_2$ at zero pressure. The data for $x = 0.18$ and $x = 0.31$ are taken from the supplementary information in Ref. 5. (a) The temperature range below 10 K, symbols - experimental data, solid lines - single band fit Eq.1, dashed lines - multiband fit Eq. 2. (b) The temperature range up to 300 K. Inset: the dependence of the exponent n vs. the residual resistivity ρ_0 , see Eq. (1). The data for $K_{1-x}Na_xFe_2As_2$ crystals ($x \neq 0$) are taken from the supplementary information in Ref. 5, for $x = 0$ (open rhombus) from Ref. 23. The solid line is a guide-to-the-eye.

procedure as proposed in Ref. 8. In this way, the resistivity data $\rho(T)$ of each sample were multiplied by a factor $\langle \rho(300K) \rangle / \rho(300K)$, where $\rho(300K)$ is the measured resistivity of the sample at $T = 300$ K and $\langle \rho(300K) \rangle = 0.36$ m Ω cm is our average resistivity value over all of our samples at $T = 300$ K. Below we show only normalized $\rho(T)$ data. To fit the data below 15 K, we used the standard single-band expression

$$\rho(T) = \rho_0 + AT^n. \quad (1)$$

The obtained residual resistivity ρ_0 monotonically increases with the Na doping level as shown in Fig.1a. In turn, T_c decreases with the increasing ρ_0 in accord with the presence of the disorder induced pair-breaking.⁵ We have found that the exponent n is always below 2:

x	$\rho_{01}(\mu\Omega\text{cm})$	$\rho_{02}(\mu\Omega\text{cm})$	$A_1(\mu\Omega\text{cm}/\text{K}^2)$	$A_2(\mu\Omega\text{cm}/\text{K}^2)$
0 (S1)	0.6	0.6	0.024	0.25
0.18	1.9	1.2	0.021	0.25
0.31	7	5.5	0.021	0.25

TABLE I: The parameters of the two-band analysis of the normal state resistivity below $T = 15$ K.

$n \approx 1.8$ for our stoichiometric K-122 samples and it decreases to $n \approx 1$ for the single crystals with a high Na substitution level. In the case of single-band materials such a deviation from a T^2 dependence would signal a non-Fermi liquid (nFL) behavior. For example, the deviation from the FL behavior in the strongly disordered K-122 has been interpreted as evidence for quantum criticality⁴³. However, in a multiband system, which K-122 is, the deviation from the T^2 behavior can be observed even in the case when all i bands behave like $\rho(T)_i = \rho_{0i} + A_i T^2$. For the resulting resistivity of the multiband system we have:

$$\rho(T) = \left[\sum_i (1/\rho_i(T)) \right]^{-1}. \quad (2)$$

Strictly speaking, in the case of K-122 a four (five) band-model should be considered, if one neglects (takes into account) the small 3-dimensional band near the Z point of the BZ (see Fig.7) with 8(10) independent parameters. To demonstrate that the data can be fitted by Eq.2 we considered for the sake of simplicity an effective two-band model as shown in Fig.1a. (The details of the fitting parameters are given in Table I.) As can be seen, a two-band analysis results in quite different A_i values. The value of the coefficient A_1 is close to the values reported for K-122 compounds obtained using the single-band Eq. 1.^{14,19} However, the value of the coefficient A_2 is about one order of magnitude larger than that of A_1 . This difference can be understood if we consider that $A \propto n/N_0(0)^2 \langle v_{ab}^2 \rangle \omega^{*2}$, where n is the density of the carriers, $N_0(0)$ is the bare density of states (DOS) at the Fermi energy, v_{ab} is the bare Fermi velocity in the ab plane, and ω^* is the frequency which determines the magnitude of the frequency dependent term in the imaginary part of the self-energy and contains all of the many-body effects.⁴⁴ Then, the ratio $A_2/A_1 \sim 10$ can be explained by the ratio of $\omega_1^{*2}/\omega_2^{*2}$, only, by taking into account rather different band dependent quasiparticle effective masses for K-122^{3,4}. Therefore, the obtained parameters (see Table I) have reasonable values for the $K_{1-x}Na_xFe_2As_2$ system under consideration which suggests that the nominally nFL behavior of the total $\rho(T)$ can be explained by a multiband effect with all bands in a FL state.

Fig. 2 shows the T dependence of the magnetization for $K_{1-x}Na_xFe_2As_2$ single crystals. The T_c for the samples is defined using linear extrapolations as shown in Fig. 2.

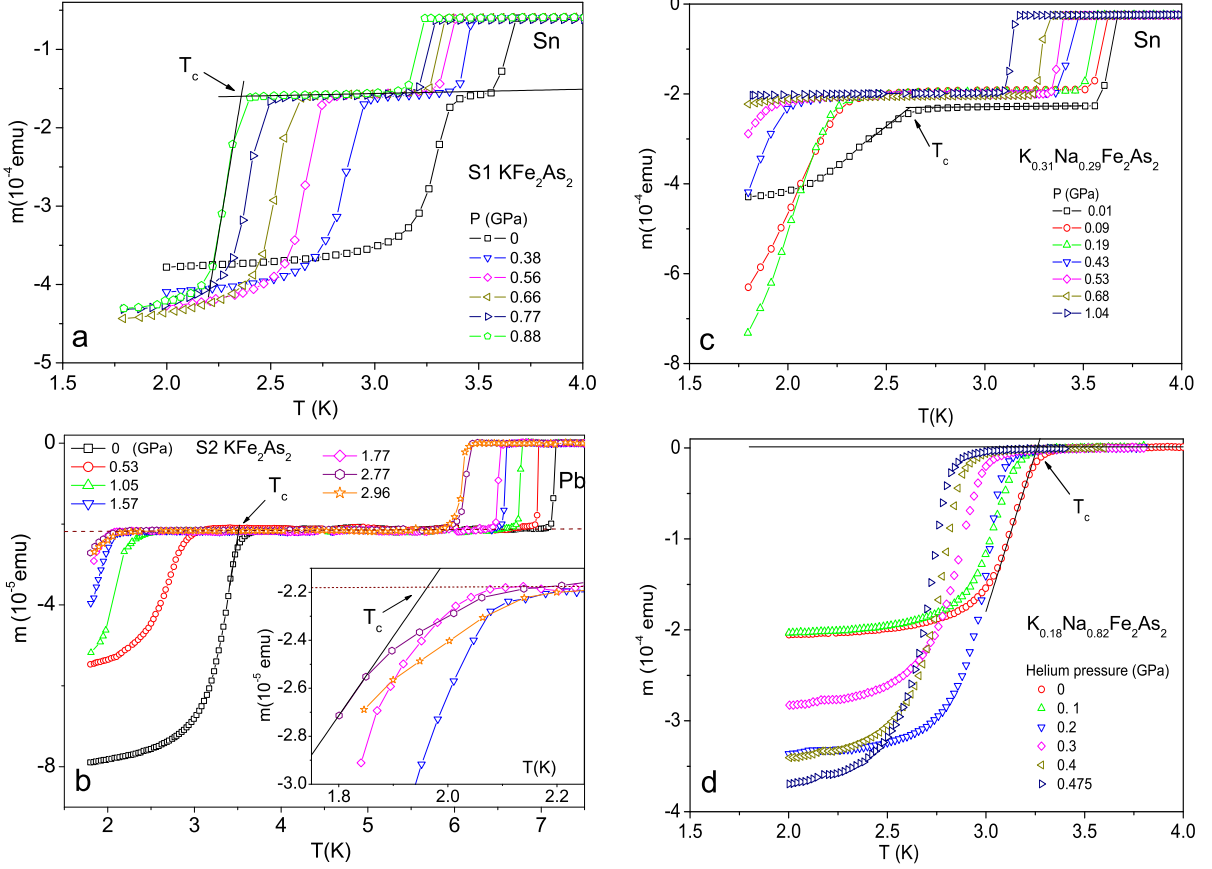


FIG. 2: (color online) The T dependence of the magnetization of $K_{1-x}Na_xFe_2As_2$ measured in 10 Oe at different applied pressures. The second superconducting transition at higher temperature (Figs. a, b, and c) corresponds to a low-temperature pressure gauge such as Sn or Pb. a) $x = 0$ (S1 sample) measured in a Quantum Design pressure cell. b) $x = 0$ (S2 sample) measured in a home-made pressure cell. Inset: zoom to the data at high pressure. c) Sample with $x = 0.31$ measured in a Quantum Design pressure cell, d) Sample with $x = 0.18$ measured in a He gas pressure cell. The data in Fig. b, d were corrected for the background signal.

Using this criterion for the critical temperature similar T_c values are obtained from our magnetization data and from specific heat measurements performed on the crystals from the same batch^{30,31}. This T_c criterion results in slightly lower T_c values than that obtained from the zero-resistivity value usually used as a criterion for T_c in the transport measurements under pressure.^{2,19} However, the observed small discrepancy between these two criteria does not affect the main conclusion of our work. It is seen in Fig. 2 that T_c of all samples monotonically decreases with pressure up to about 2 GPa. The sample S2 ($x = 0$) was measured up to the maximum pressure of about 3 GPa Fig. 2b. It is seen in Fig. 3a that the pressure dependence of T_c for this sample has a shallow minimum at about 2 GPa in accord with the data obtained in the experiments with He as a pressure medium.¹⁹

The pressure dependence of T_c for our $K_{1-x}Na_xFe_2As_2$ system and the available data in the literature for K-122,^{1,2,17,19,21} Cs-122²¹ and Rb-122²⁶ are summarized in Fig. 3a. One can see that $K_{1-x}Na_xFe_2As_2$ and stoichiometric K-122 with different T_c values at zero pressure ex-

hibit a similar pressure derivative $dT_c/dP \approx -1$ K/GPa. However, the sister compounds Rb-122 and Cs-122 show clearly different pressure derivatives -1.35 K/GPa and -0.85 K/GPa, correspondingly. As was shown in our previous work, the T_c of the $K_{1-x}Na_xFe_2As_2$ system at zero pressure is defined mainly by a single strongly coupled superconducting band.⁵ To demonstrate that the Na substitution suppresses T_c due to the pair-breaking effect, only, and that it does not affect the superconducting coupling constants λ we analyzed our experimental data adopting the single-band Abrikosov-Gor'kov (AG) formula modified for the d -wave case⁴⁵

$$-\ln\left(\frac{T_c}{T_{c0}}\right) = \psi\left(\frac{1}{2} + \frac{\alpha T_{c0}}{2\pi T_c}\right) - \psi\left(\frac{1}{2}\right), \quad (3)$$

where $\alpha = 1/[2\tau_{\text{eff}}T_{c0}]$ is the pair-breaking parameter and $1/\tau_{\text{eff}} \propto \rho_0$ is the effective scattering rate due to impurities created by the Na substitution. The quantities τ_{eff} , and T_{c0} can be pressure dependent. Taking this into account, we have found that all available data for the $K_{1-x}Na_xFe_2As_2$ system and the disordered K-122 crys-

x	$T(K)$	a (Å)	c (Å)	z_{As}
0.37(10)	300	3.8341(2)	13.656(2)	0.3541(1)
0.37(10)	300	3.8353(3)	13.693(2)	0.3541(2)
0.22(0.12)	100	3.8172(5)	13.596(2)	0.35461(18)

TABLE II: The crystal structure parameters of $K_{1-x}Na_xFe_2As_2$ single crystals. The values for the partially Na substituted samples have been obtained from x-ray data. The x values are in a reasonable agreement with EDX data (0.31 and 0.18) obtained on the crystals from the same batches.

tals can be fitted by the AG formula assuming that the critical temperature of the clean system (without pair-breaking impurities) varies linearly with pressure and can be approximated by $T_{c0}(P) = 3.56 \text{ K} - 1.11P$ up to $P \approx 1.5$ GPa. In contrast, it is found that τ_{eff} is pressure independent. In general, the observed AG behavior in the $K_{1-x}Na_xFe_2As_2$ system may be considered as a justification that Na acts as a pair-breaking impurity in agreement with Ref. 5.

The independence of $T_{c0}(P)$ on the Na concentration is illustrated in Fig. 3b, where we plot the normalized $T_c/T_{c0}(P)$ versus the residual resistivity ρ_0 measured at zero pressure divided by $T_{c0}(P)$. It is seen that all available data up to 1.5 GPa scale on a single curve. The observed scaling indicates, also, that both τ_{eff} and $\rho_0 \propto 1/\tau_{eff}$ is nearly pressure independent. The insensitivity of ρ_0 to pressure for K-122 is confirmed experimentally.²⁸ Interestingly, the Cs-122 data can be scaled to the same curve using their different $T_{c0}(P) = 2.8K - 0.85P$, only. Note, that the clean limit $T_{c0}(P = 0) = 2.8$ K is rather reasonable for Cs-122 compound taking into account available literature data.²¹⁻²³. For example, the reported in Ref. 22 $T_c \approx 2.6$ K is quite close to our adopted $T_{c0}(P = 0)$ value.

B. Crystal structure

It is well known that isovalent chemical substitution in iron pnictides suppresses the SDW phase and can induce superconductivity (see for example Refs. 46,47). In this case one of the relevant factors which controls the phase diagram is the change of the structure parameters⁴⁸. This effect can be considered as a chemical pressure. To understand the effect of the Na substitution on the lattice parameters, we performed single crystal diffraction measurements at room temperature and at $T = 100$ K. Selected crystallographic results are given in Table II. The lattice parameters of $K_{1-x}Na_xFe_2As_2$ single crystals obtained at $T = 300$ K are compared with the experimental data for K-122²¹ obtained at room temperature (Fig. 4a) and the lattice parameters obtained at $T = 100$ K are compared with the results

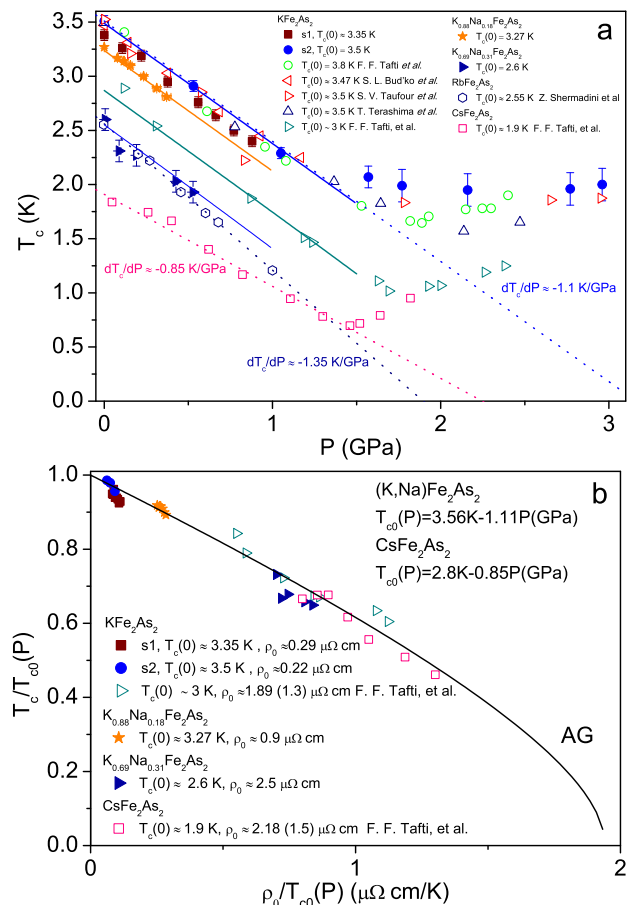


FIG. 3: (color online) a) The pressure dependence of T_c for $K_{1-x}Na_xFe_2As_2$ samples from this work and those taken from the literature for stoichiometric K-122^{1,2,17,19,21}, Cs122²¹, Rb122²⁶. Dashed lines: linear fit and solid lines: results obtained from Eq. 3. b) The normalized critical temperature $T_c/T_{c0}(P)$ vs. the ratio between the residual resistivity at zero pressure and the critical temperature for clean K-122 $\rho_0/T_{c0}(P)$. The solid line denotes the Abrikosov-Gor'kov formula. The ρ_0 values for disordered K-122 and Cs-122 samples (in brackets) are taken from Ref. 21 and have been normalized according to procedure described in the text.

of our DFT calculations relevant for low temperature (Fig. 4b). We note that the lattice parameters only weakly depend on temperature below $T \sim 100$ K⁴⁹. It is seen in Fig. 4 that the chemical pressure due to the Na substitution produces a stronger effect along the c axis by about a factor of 2 - 3 than in the ab plane as compared to the hydrostatic external pressure effect on K-122. Taking into account that T_c of K-122 is equally sensitive to uniaxial pressure applied in the ab plane and along the c axis ($\partial T_c/\partial P_{ab} \approx -\partial T_c/\partial P_c$) with the resulting superposed pressure derivative $dT_c/dP = 2\partial T_c/\partial P_{ab} + \partial T_c/\partial P_c$ ¹⁷, we can conclude that the chemical pressure effect on T_c due to the Na substitution is rather weak.⁵⁰ This provides additional support for our assumption that the main reason of the

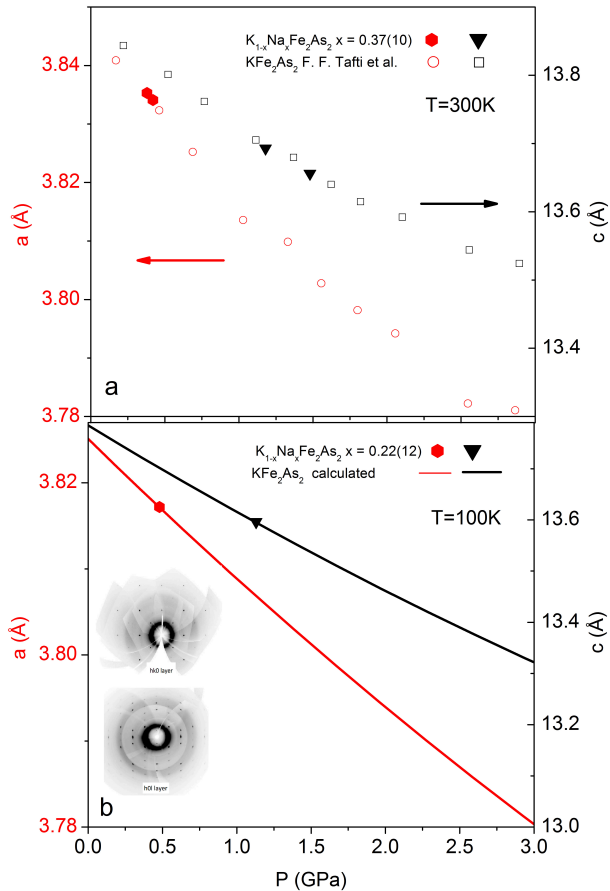


FIG. 4: (color online) The hydrostatic pressure dependence of the lattice parameters for K-122. The experimental data for K-122 are taken from Ref. 21. The data points for $K_{1-x}Na_xFe_2As_2$ correspond to the lattice parameters which have been obtained from x-ray data at atmospheric pressure. The data points are shifted along the pressure axis to fit the values for KFe_2As_2 at external hydrostatic pressure. a) The data obtained at room temperature. Close symbols - the experimental data for $K_{1-x}Na_xFe_2As_2$, open symbols are taken from Ref.²¹ b) Close symbols - the experimental data for $K_{1-x}Na_xFe_2As_2$ obtained at $T \approx 100$ K. Solid lines - theoretical calculations corresponding to the low-temperature regime. Inset: single crystalline diffraction pattern of (hk0), and (h0l) planes for a Na doped crystal.

observed T_c suppression in Na doped crystals is given by the pair-breaking effect.

IV. THEORETICAL ANALYSIS

To get a better understanding of the pressure effect on T_c we performed a density functional theory (DFT) based theoretical analysis of the band structure under pressure.

	a (Å)	b (Å)	c (Å)	z_{As}
EXP	3.83	3.83	13.79	0.353
PM	3.79	3.79	13.99	0.346

TABLE III: Experimental⁴⁹ and paramagnetic fully optimized structural parameters of KFe_2As_2 .

A. Computational details

The calculations were performed using the Vienna Ab-Initio Simulation Package (VASP)^{51,52} within the generalized gradient approximation (GGA)⁵³. The Perdew, Burke and Ernzerhof (PBE)⁵⁴ functional was used to calculate the exchange-correlation potential. We used projected augmented-wave (PAW) pseudopotentials⁵⁵ for all the atomic species involved, and in order to achieve a satisfactory degree of convergence the integrations over the Brillouin Zone (BZ) was performed considering $12 \times 12 \times 8$ and $24 \times 24 \times 24$ uniform Monkhorst and Pack⁵⁶ grids for the conventional (4 K, 8 Fe and 8 As atoms) and single formula unit (1 K, 2 Fe and 2 As atoms) cells, respectively, and energy cutoff up to 500 eV. The Fermi surface cuts of chosen lattice structures (see below) as a function of k_z have been computed using a $64 \times 64 \times 4$ k-points grid.

B. Band structure and Fermi surfaces

We studied the influence of the structural properties on the electronic paramagnetic (PM) band structure of KFe_2As_2 . In Fig. 5, we report the calculated band structure considering the experimental⁴⁹ and the optimized lattice constants in the PM phase. The predicted (theoretical) and experimental lattice constants are compared in table III. In spite of relatively small differences between experimental and theoretical lattice parameters (in a range of 1 - 2 %), the Fermi surface cross-sections calculated with experimental lattice parameters reveal important differences with respect to the theoretical calculated ones. The radii of the Γ -centered hole Fermi surfaces, namely α , ζ and β , do not change sensibly, while the small electron-pockets around the X point shrink considering the theoretical lattice constants. The small (but irrelevant) electron pocket at Z is found to become larger using the theoretical lattice parameters. Since the discrepancy between theoretical and experimental crystal lattices affects bands, in the further analysis we stick to the experimental structure⁴⁹: we consider this one as the reference geometry at $P = 0$, i. e., $z_{As}^{exp} = z_{As}(P = 0)$, $a^{exp} = a(P = 0)$, and $c^{exp} = c(P = 0)$. Then, we extracted the lattice parameters calculating the compressibility for the $z_{As}^{th}(P)$, $a^{th}(P)$ and $c^{th}(P)$ by first principles as a function of the pressure. The lattice con-

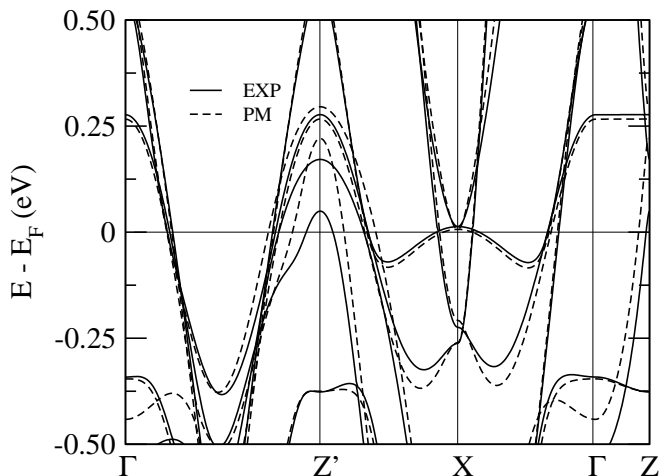


FIG. 5: KFe_2As_2 band structure considering different crystal lattice parameters (namely, the experimental and PM ones, see table III).

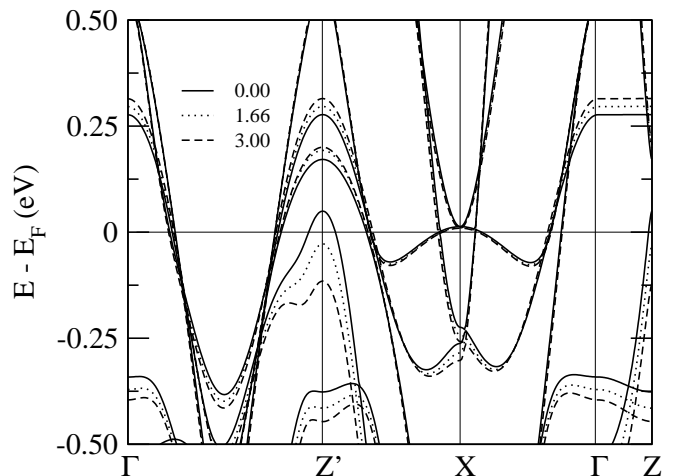


FIG. 6: KFe_2As_2 band structure for the experimental lattice structure (taken as $P = 0$ GPa geometry) and lattice parameters extrapolated with compressibility at 1.66 and 3.00 GPa (see Tab. IV).

stants, obtained in this way, are given in Tab. IV. These data was also used for the analysis of the chemical pressure (see Fig. 4b). The calculated band structure and Fermi surface cross-sections with these lattice parameters are given in Figs. 6, and 7 for different pressures. We underline that experiments found the two outermost FSS around the Γ point not intersecting³, however, DFT-GGA find them crossing. Keeping into account this effect on the band structure, the orbital character of the Fermi Surface is the following: *i*) the main contribution to the α FS is from d_{z^2} (along the ΓZ direction) and from d_{xz+yz} (along the ΓX direction) orbitals; *ii*) we call ζ the band with character d_{xy} (the green FS along the ΓZ direction which becomes red along the ΓX , see Fig. 7); *iii*) in the same way, we refer to β the FS with d_{xz+yz} character (the outermost red FS along the ΓZ direction becoming the middle green one along ΓX , see Fig. 7); *iv*) the main contribution to the lobes ϵ near the X point is from d_{xz+yz} and d_{xy} ; *v*) the character of the three dimensional FS at the Z point (orange band in Fig. 7) is d_{xy} .

In order to understand the origin of the reversed behavior of T_c under pressure, first, we compared the band structure at ambient ($P = 0$ GPa), close to the critical pressure ($P = 1.66$ GPa) and at high pressure ($P = 3$ GPa), shown in Fig. 6. The shape of the relevant Fermi surfaces are not strongly affected in this range of pressure, indicating that the origin of the non-monotonic pressure dependence of T_c is not due to changes of the Fermi surface topology in accord with experimental findings.^{1,2}

V. DISCUSSION

The total density of states (TDOS) for different values of pressure is presented in Fig. 8. At zero pressure TDOS has a minimum at energies of a few meV above

P (GPa)	a (Å)	c (Å)	z_{As}	z_{As} (Å)
0.00	3.83	13.79	0.353	1.42
1.00	3.81	13.62	0.355	1.42
1.66	3.80	13.51	0.356	1.43
2.00	3.80	13.45	0.356	1.43
2.50	3.79	13.37	0.357	1.43
3.00	3.78	13.28	0.358	1.43
4.00	3.76	13.11	0.359	1.43

TABLE IV: Structural parameters for the four different pressure values ($P = 0$ GPa is relative to the experimental cell taken as reference, see text).

the Fermi level, which is followed by a peak in TDOS. Applying pressure leads to a redistribution of the states, that formally looks like Fermi level moves up through the minimum towards the sharp peak. As a result TDOS at the Fermi-level first decreases with the pressure, has a minimum at the pressure of about 2 GPa and increases back as shown in the inset of Fig. 8.

The change of the DOS may affect T_c . As it was shown from thermodynamics, in the clean limit the T_{c0} of K-122 is determined mainly by a single band.^{5,8,11} For further discussion we adopt the model proposed in Ref. 5 with coupling constants $\lambda_z \approx 0.9$ and $\lambda_\phi \approx 0.8$. In this case the critical temperature can be written as $\ln(\omega_b/T_{c0}) = (1 + \lambda)/a\lambda$, where ω_b is the characteristic bosonic frequency of the superconducting "glue", $\lambda = \lambda_z \approx 0.9$ is the coupling constant and $a = \lambda_\phi/\lambda_z \approx 0.9$. Then, assuming that ω_b and a are pressure independent, for the pressure dependence of T_c we have

$$T_{c0}(P) \approx T_{c0}(0) \frac{\exp(-\frac{1+\lambda(P)}{a\lambda(P)})}{\exp(-\frac{1+\lambda(0)}{a\lambda(0)})}. \quad (4)$$

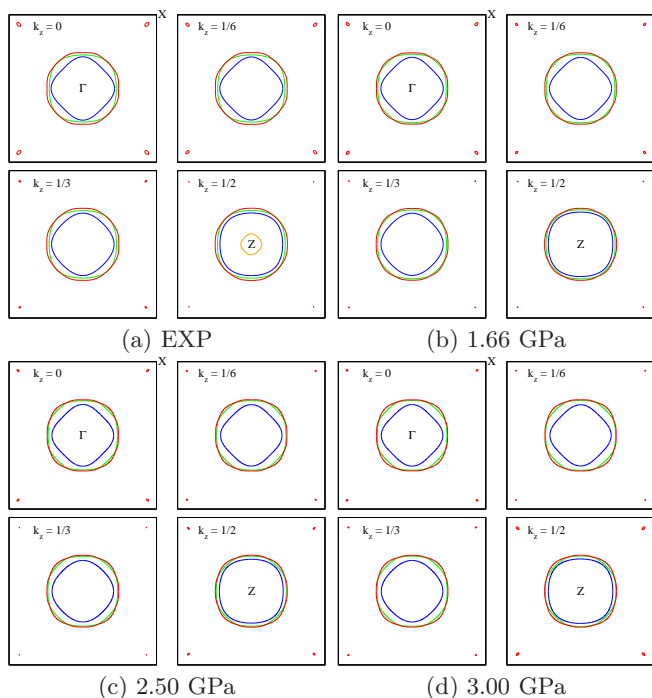


FIG. 7: (color online) Fermi surfaces cuts along the positive k_z direction for KFe_2As_2 for the experimental crystal structure and for the extrapolated lattice parameters using the predicted compressibility. The inner, middle and outer FS's around the Γ -point are identified as α , ζ and β , respectively. (For the orbital content of FS's see text.)

Taking into account that $\lambda = gN_i$, with g as the effective interaction and N_i as the partial density of states (PDOS) of the leading superconducting band, then for small variations of g and N the variation of the critical temperature under pressure can be written as

$$\frac{\delta T_{c0}}{T_{c0}} \approx \frac{1}{a\lambda} \left[\frac{\delta g}{g} + \frac{\delta N_i}{N_i} \right]. \quad (5)$$

As shown in Fig. 9 the partial density of states (PDOS) of the various FSSs behave differently with pressure. $N_\alpha(0)$ weakly depends on pressure up to 4 GPa while $N_{\beta+\zeta}(0)$ decreases from 0 to 1.66 GPa by about 20% and then remains practically constant. At this point, it is clear that the weak increase of the TDOS above 2 GPa (Fig. 8) comes mainly from the ϵ band. Indeed, the $N_\epsilon(0)$ increases up to 4 GPa as it can be seen in Fig. 9. The non-monotonic pressure dependence of $N_{\beta+\zeta}(0)$ resembles the experimentally observed $T_{c0}(P)$ dependence (Fig. 3). Using Eq. 4 one can estimate from $N_{\beta+\zeta}(0)$ that it corresponds to a decrease of the critical temperature from $T_c(P=0) \approx 3.5$ K down to $T_c(P=1.66 \text{ GPa}) \sim 2.5$ K assuming that g is pressure independent. However, within a more quantitative study the change of the pairing interaction g (see Eq. 5) and of the spin-fluctuation spectrum, i.e., ω_b , under pressure should be taken into account, too. Above $P = 1.66$ GPa T_c would remain nearly constant. This is consistent with a broad mini-

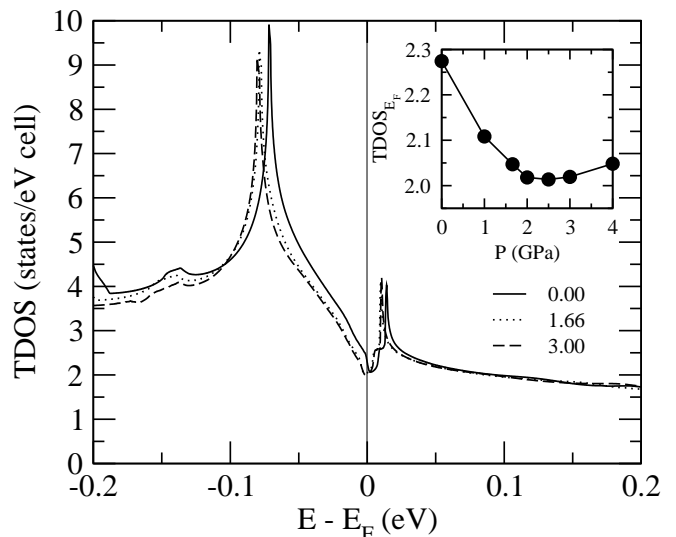


FIG. 8: The variation of the total density of states (TDOS) under pressure for KFe_2As_2 (per one spin). Inset: pressure dependence of the TDOS at the Fermi level.

imum in the pressure dependence of T_c reported in Refs. 1,19 and observed in our data, too (see Fig. 3). Note, that due to the overlap of the β (mainly of $xz + yz$ orbital content) and ζ (mainly of xy orbital content) FSSs we could not separate them unambiguously. However, as shown in Fig. 10 the orbital-projected PDOS for all bands except $xz + yz$ decreases in the whole pressure range. Therefore, based on our theoretical analysis we suggest that the experimentally observed non-monotonic pressure dependence of T_c is related to the $xz + yz$ band. Then, the β FSS, predominantly having $xz + yz$ character (experimentally the middle ζ FSS⁹), is responsible for the superconductivity in the K-122 compound. We note, that the presence of a nodal SC gap of about 0.7 meV (as estimated from our specific heat data⁵) on the middle FSS is in a quantitative agreement with the laser ARPES experiments.⁹ However, the observed very large nodeless SC gap on the inner FSS⁹ disagrees with the specific heat data. Therefore, further investigations are required to understand this discrepancy.

In this context, the observed AG-type scaling of the pressure dependencies of T_c for nodal K,Na-122 and Cs-122 suggests that these compounds have the same superconducting gap symmetry. However, the Cs-122 and the (K,Na)-122 systems have different T_{c0} and hence different coupling constants. In the case of extended s -wave pairing symmetry such as s_{\pm} -wave SC with accidental nodes, the nodal position is not fixed on the Fermi surface^{8,57,58}. Therefore, nodes can be lifted by impurities, pressure or isovalent substitution. In some cases a reentrant behavior of the nodes can be observed.⁵⁸ In contrast, for K,Na-122 single crystals we observed a monotonic increase of the residual electronic specific heat C_{el}/T with Na substitution and a nearly Na independent T^2 behavior of

Band	k_z	FS area (BZ %)					FS frequencies (kT)					m^*/m_e		
		dHvA ^{a,c}	A. ^a	A. ^b	LDA ^a	GGA	dHvA ^c	QOM ^d	LDA ^e	DMFT ^f	GGA	dHvA ^c	A. ^a	GGA
α	Γ	8.2	9.1	7	12.2	12.7	2.30	2.31	3.42	4.05	3.56	6.0	5.1	1.43
	Z	8.6	9.8	7	13.8	15.0	2.39	2.39	3.86	4.20	4.20	6.5	6.6	2.92
ζ	Γ	10.3	12.2	-	16.7	17.5	2.89	2.89	4.67	0.94	4.93	8.5	11.0	2.43
	Z	15.7	17.0	-	17.4	17.8	4.40	4.40	4.88	3.25	5.01	18.0	17.7	2.47
β	Γ	25.6	27.3	22	20.8	19.2	7.16	7.18	5.82	6.62	5.39	19	16.3	2.42
	Z	-	30.0	22	21.6	19.2	-	-	6.03	6.81	5.40	-	17.9	2.35
ϵ	Γ	0.86	2.1	2.5	0.36	0.157	0.24	0.24	0.03	-	0.02	6.0	5.6	0.30
	Z	1.29	2.1	2.5	0.11	0.003	0.36	0.36	0.10	0.42	0.03	7.2	4.1	0.41

TABLE V: Cross sectional areas, dHvA frequencies and effective masses obtained by different experimental and theoretical techniques: A.= ARPES, QOM= Quantum Oscillations in Magnetostriction. The areas are expressed in term of the % area occupied of the 2D BZ. The dHvA frequencies are expressed in kT. Our calculations are shown in the ‘‘GGA’’ columns. ^aRef. 60, ^bRef. 61, ^cRef. 3, ^dRef. 62, ^eRef. 63, ^fRef. 64. Note, that strong electronic correlations are neglected in LDA and GGA calculations. These correlations presumably cause the inversion of β and ζ bands in the experiment, see for example Refs. 10,64.

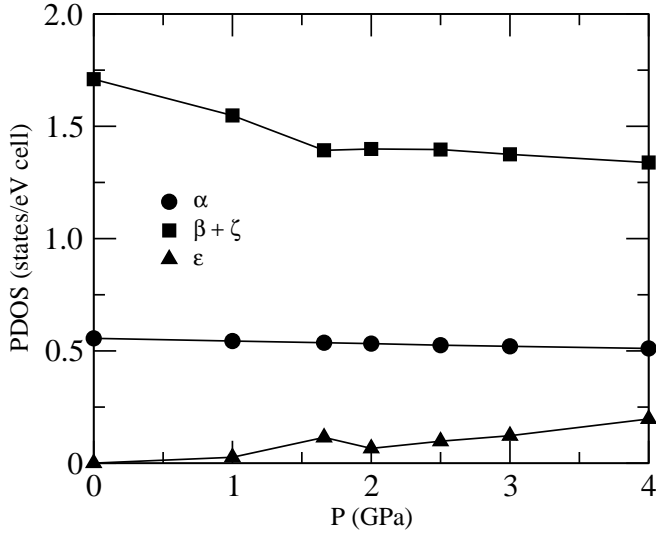


FIG. 9: The variation of the band-resolved DOS at the Fermi level under pressure for KFe_2As_2 .

Band	Pos.	0 GPa	1.66 GPa	2.50 GPa	3.00 GPa
α	inner	3.56	3.54	3.49	3.47
		4.20	4.58	4.51	4.60
ζ	middle	4.93	5.16	5.27	5.31
		5.01	5.24	5.35	5.38
β	outer	5.39	5.49	5.56	5.59
		5.40	5.51	5.60	5.66

TABLE VI: Low (top row) and high (bottom row) dHvA frequencies (kT) as a function of the pressure for different FS bands. The band position is indicated in the second column.

C_{el} at low-temperature.^{5,7} Therefore, our data are consistent with a symmetry protected d -wave SC in these compounds which is stable at least up to the pressure where T_c has a minimum (see Fig. 3b).

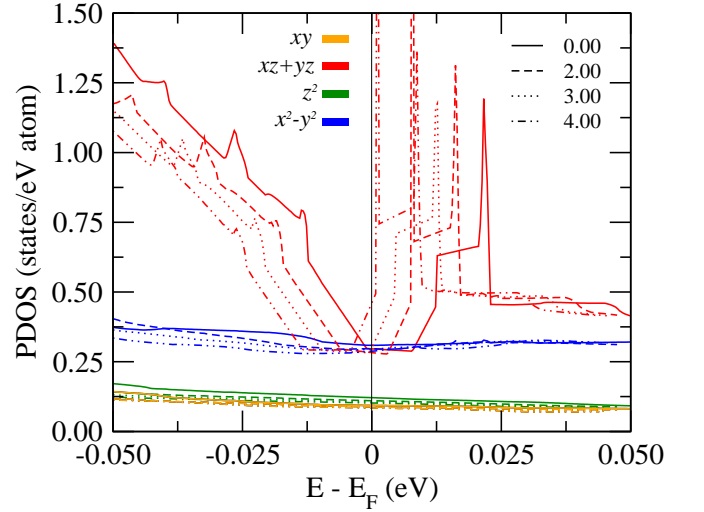


FIG. 10: The variation of the various Fe 3d orbitals projected density of states under pressure for KFe_2As_2 per spin and one Fe atom.

Finally, we compare the calculated Fermi surface cross sections with the experimental ones obtained from dHvA measurements¹. These dHvA experiments show, that the size of the lobes near the X-point decreases with pressure and that of the α cylinder weakly increases up to 2.47 GPa, the maximum pressure reached experimentally. The trend in the calculated Fermi surface cross sections for this pressure range, i.e. up to 2.5 GPa (see Fig. 7) is consistent with the corresponding dHvA frequencies. However, increasing the pressure above 2.5 GPa, e.g. in the case of 3 GPa shown in Fig. 7(d), the size of the lobes maintain their dimension. Thus, this prediction could be verified experimentally by studies around this pressure.

For this purpose, in Tab. V we collected the calculated cross section of various FS bands, dHvA frequencies and the m^*/m_e ratios as found in the literature from both measurements and simulations. Together with them, we

add our GGA results calculated for the experimental crystal structure. The dHvA frequencies and the m^*/m_e -ratio have been estimated calculating the extremal FS areas and the relative orbit frequencies using its implementation in the SKEAF code⁵⁹. The GGA calculated FS cross sections are in qualitative agreement with respect to the experiments (except ϵ FS). However, the theoretical m^*/m_e ratios essentially underestimate experimental values pointing to sizable correlation effects in accord with a previous study. In this context we note that the observed large difference of the effective resistivity coefficients A_1 and A_2 discussed above (see Tab.I), is likely to be caused by the high-energy mass renormalizations and not related directly to the pairing interactions. This suggestion is also consistent with the significant pressure dependence of the approximate effective single A coefficient reported by V. Taufour *et al.*¹⁹.

At this point, we extended the study to high pressure and we report the results of calculated dHvA frequencies and we compared them with experimental measurements.¹ The results obtained in the calculations are shown in Tab. VI for the FS's shown in Fig. 7. We observed that the largest dHvA frequency increases for the α -band as a function of the pressure, in agreement with experiment.¹ At the same time, the lowest frequency slightly decreases with pressure overestimating the increase of the three dimensionality of the electronic structure under pressure as compared to experiment.¹

We confirm, moreover, the absence of a Lifshitz transition under pressure.⁶⁵ Note, that the variation of the TDOS at the Fermi level in the pressure range up to 3 GPa is below 15% as shown in Fig. 8. Such a relatively small variation of the TDOS for multiband systems can be hardly distinguished in experiments such as transport measurements. Therefore, we suppose that the observation of a nearly pressure independent Hall coefficient and residual resistivity^{2,28} cannot exclude such relatively small variations of the DOS.

VI. CONCLUSION

In conclusion, we investigated the effect of hydrostatic pressure and Na substitution on the superconducting and the normal-state properties of KFe_2As_2 . We have found that the Na substitution noticeably affects the lattice

parameters which can be considered as a non-hydrostatic chemical pressure. However, the comparison of the external hydrostatic pressure with the chemical pressure shows that the total effect of the structural changes on T_c due to Na substitution is rather weak. Therefore, the main mechanism of the T_c suppression in Na doped crystals is a weak pair-breaking effect caused by disorder. The Na substitution enhances the residual resistivity and leads to a formal non-Fermi liquid behavior in the temperature dependence of the resistivity. We have shown that this deviation from the T^2 behavior can be described by multiband effects due to different effective quasi-particle masses for different bands. The pressure dependencies of T_c for the $\text{K}_{1-x}\text{Na}_x\text{Fe}_2\text{As}_2$ system can be described by the single-band Abrikosov-Gor'kov-type scaling curve using the Na independent critical temperature in a clean limit $T_{c0}(\text{P})$. These observations additionally confirm that the T_c suppression for Na substitution is mainly caused by the pair-breaking effect. The pressure dependence of T_c for CsFe_2As_2 can be also scaled on the same curve, however, with a different $T_{c0}(\text{P})$. These results suggest the same pairing symmetry for this compound as for the $\text{K}_{1-x}\text{Na}_x\text{Fe}_2\text{As}_2$ system. Additionally, we performed theoretical investigations of the band structure of KFe_2As_2 under pressure within the generalized gradient approximation. Our results suggest, that the observed pressure dependence of T_c can be explained by the non-monotonic variation of the PDOS of the $xz + yz$ derived band under pressure without a change of the pairing symmetry. This $xz + yz$ derived band is supposed to be most relevant for the superconductivity of the $\text{K}_{1-x}\text{Na}_x\text{Fe}_2\text{As}_2$ system.

Acknowledgment

This work was supported by the EU-Japan project (No. 283204 SUPER-IRON), and the DFG through the SPP 1458, the E.-Noether program (WU 595/3-1 (S.W.)). S.W. thanks the BMBF for support in the frame of the ERA.Net RUS project FeSuCo No. 245, E.A. thanks the DFG-GRK1621 and I.M. thanks funding from RFBR (12-03-01143-a). We acknowledge D. Evtushinsky, K. Iida, K. Nenkov, C. Hess, and A. Yaresko for fruitful discussion.

* Electronic address: v.grinenko@ifw-dresden.de

‡ Electronic address: fabio.ricci@aquila.infn.it

¹ T. Terashima, K. Kihou, K. Sugii, N. Kikugawa, T. Matsumoto, S. Ishida, C.-H. Lee, A. Iyo, H. Eisaki, and S. Uji, *Phys. Rev. B* **89**, 134520 (2014).

² F.F. Tafti, A. Juneau-Fecteau, M.-. Delage, S. Ren de Cotret, J.-P. Reid, A.F. Wang, X.-G. Luo, X.H. Chen, N. Doiron-Leyraud, and L. Taillefer, *Nature Physics* **9**, 349

(2013).

³ T. Terashima, N. Kurita, M. Kimata, M. Tomita, S. Tsuchiya, M. Imai, A. Sato, K. Kihou, C.-H. Lee, H. Kito, H. Eisaki, A. Iyo, T. Saito, H. Fukazawa, Y. Kohori, H. Harima, and S. Uji, *Phys. Rev. B* **87**, 224512 (2013).

⁴ F. Hardy, A.E. Böhmer, D. Aoki, P. Burger, T. Wolf, P. Schweiss, R. Heid, P. Adelmann, Y.X. Yao, G. Kotliar, J. Schmalian, and C. Meingast, *Phys. Rev. Lett.* **111** 027002

- (2013).
- ⁵ V. Grinenko, D.V. Efremov, S.-L. Drechsler, S. Aswartham, D. Gruner, M. Roslova, I. Morozov, K. Nenkov, S. Wurmehl, A.U.B. Wolter, B. Holzapfel, and B. Büchner Phys. Rev. B **89**, 060504(R) (2014).
 - ⁶ H. Fukazawa, T. Saito, Y. Yamada, K. Kondo, M. Hirano, Y. Kohori, K. Kuga, A. Sakai, Y. Matsumoto, S. Nakatsuji, K. Kihou, A. Iyo, C.H. Lee, and H. Eisaki, J. Phys. Soc. Jpn. **80**, SA118 (2011).
 - ⁷ M. Abdel-Hafez, V. Grinenko, S. Aswartham, I. Morozov, M. Roslova, O. Vakaliuk, S. Johnston, D.V. Efremov, J. van den Brink, H. Rosner, M. Kumar, C. Hess, S. Wurmehl, A.U.B. Wolter, B. Büchner, E.L. Green, J. Wosnitza, P. Vogt, A. Reifemberger, C. Enss, M. Hempel, R. Klingeler, and S.-L. Drechsler, Phys. Rev. B **87**, 180507(R) (2013).
 - ⁸ J.-Ph. Reid, M.A. Tanatar, A. Juneau-Fecteau, R.T. Gordon, S.R. de Cotret, N. Doiron-Leyraud, T. Saito, H. Fukazawa, Y. Kohori, K. Kihou, C.H. Lee, A. Iyo, H. Eisaki, R. Prozorov, and L. Taillefer, Phys. Rev. Lett. **109**, 087001 (2012).
 - ⁹ K. Okazaki, Y. Ota, Y. Kotani, W. Malaeb, Y. Ishida, T. Shimojima, T. Kiss, S. Watanabe, C.-T. Chen, K. Kihou, C.H. Lee, A. Iyo, H. Eisaki, T. Saito, H. Fukazawa, Y. Kohori, K. Hashimoto, T. Shibauchi, Y. Matsuda, H. Ikeda, H. Miyahara, R. Arita, A. Chainani, S. Shin, Science **337**, 1314 (2012).
 - ¹⁰ Z.P. Yin, K. Haule and G. Kotliar, Nature Materials **10**, 932 (2011).
 - ¹¹ F. Hardy, R. Eder, M. Jackson, D. Aoki, C. Paulsen, T. Wolf, P. Burger, A. Böhmer, P. Schweiss, P. Adelman, R.A. Fisher, and C. Meingasta, J. Phys. Soc. Jpn. **83**, 014711 (2014).
 - ¹² S. Kittaka, Y. Aoki, N. Kase, T. Sakakibara, T. Saito, H. Fukazawa, Y. Kohori, K. Kihou, C.-H. Lee, A. Iyo, H. Eisaki, K. Deguchi, N.K. Sato, Y. Tsutsumi, and K. Machida, J. Phys. Soc. Jpn. **83** 013704 (2014).
 - ¹³ D. Watanabe, T. Yamashita, Y. Kawamoto, S. Kurata, Y. Mizukami, T. Ohta, S. Kasahara, M. Yamashita, T. Saito, H. Fukazawa, Y. Kohori, S. Ishida, K. Kihou, C.H. Lee, A. Iyo, H. Eisaki, A.B. Vorontsov, T. Shibauchi, Y. Matsuda, Phys. Rev. B **89**, 115112 (2014).
 - ¹⁴ K. Hashimoto, A. Serafin, S. Tonegawa, R. Katsumata, R. Okazaki, T. Saito, H. Fukazawa, Y. Kohori, K. Kihou, C.H. Lee, A. Iyo, H. Eisaki, H. Ikeda, Y. Matsuda, A. Carrington, and T. Shibauchi, Phys. Rev. B **82**, 014526 (2010).
 - ¹⁵ H. Kim, M. A. Tanatar, Yong Liu, Zachary Cole Sims, Chenglin Zhang, Pengcheng Dai, T. A. Lograsso, R. Prozorov, Phys. Rev. B **89**, 174519 (2014).
 - ¹⁶ H. Ikeda, R. Arita, and J. Kunes, Phys. Rev. B **82**, 024508 (2010).
 - ¹⁷ S.L. Bud'ko, Y. Liu, T. A. Lograsso, and P. C. Canfield, Phys. Rev. B **86**, 224514 (2012).
 - ¹⁸ S.L. Bud'ko, M. Sturza, D.Y. Chung, M.G. Kanatzidis, and P.C. Canfield, Phys. Rev. B **87**, 100509(R) (2013).
 - ¹⁹ V. Taufour, N. Foroozani, J.K. Lim, M.A. Tanatar, U. Kaluarachchi, S.K. Kim, Y. Liu, T.A. Lograsso, V.G. Kogan, R. Prozorov, S.L. Bud'ko, J.S. Schilling, P.C. Canfield Phys. Rev. B **89**, 220509(R) (2014).
 - ²⁰ P. Burger, F. Hardy, D. Aoki, A.E. Böhmer, R. Eder, R. Heid, T. Wolf, P. Schweiss, R. Fromknecht, M.J. Jackson, C. Paulsen, and C. Meingast, Phys. Rev. B **88**, 014517 (2013).
 - ²¹ F.F. Tafti, J.P. Clancy, M. Lapointe-Major, C. Collignon, S. Faucher, J. Sears, A. Juneau-Fecteau, N. Doiron-Leyraud, A.F. Wang, X.G. Luo, S. Desgreniers, Young-June Kim, X.H. Chen, and L. Taillefer, Phys. Rev. B **89**, 134502 (2014).
 - ²² K. Sasmal, B. Lv, B. Lorenz, A. M. Guloy, F. Chen, Y.-Y. Xue, and C.-W. Chu, PRL **101**, 107007 (2008).
 - ²³ A.F. Wang, S.Y. Zhou, X.G. Luo, X.C. Hong, Y.J. Yan, J.J. Ying, P. Cheng, G.J. Ye, Z.J. Xiang, S.Y. Li, and X. H. Chen, Phys. Rev. B **89**, 064510 (2014).
 - ²⁴ Z. Bukowski, S. Weyeneth, R. Puzniak, J. Karpinski, B. Batlogg Physica C **470**, S328 (2010).
 - ²⁵ Z. Shermadini, J. Kanter, C. Baines, M. Bendele, Z. Bukowski, R. Khasanov, H.-H. Klauss, H. Luetkens, H. Maeter, G. Pascua, B. Batlogg, and A. Amato PHYSICAL REVIEW B **82**, 144527 (2010).
 - ²⁶ Z. Shermadini, H. Luetkens, A. Maisuradze, R. Khasanov, Z. Bukowski, H.-H. Klauss, and A. Amato, Phys. Rev. B **86**, 174516 (2012).
 - ²⁷ Z. Zhang, A. F. Wang, X. C. Hong, J. Zhang, B. Y. Pan, J. Pan, Y. Xu, X. G. Luo, X. H. Chen, and S. Y. Li, arXiv:1403.0191 (2014).
 - ²⁸ F.F. Tafti; private communication. Up to 3 GPa the residual resistivity remains almost constant within deviations of about 5 % .
 - ²⁹ S.L. Bud'ko, Ni Ni, and P.C. Canfield, Phys. Rev. B **79**, 220516R (2009).
 - ³⁰ M. Abdel-Hafez, S. Aswartham, S. Wurmehl, V. Grinenko, C. Hess, S.-L. Drechsler, S. Johnston, A.U.B. Wolter, and B. Büchner, H. Rosner, L. Boeri, Phys. Rev. B **85**, 134533 (2012).
 - ³¹ V. Grinenko, S.-L. Drechsler, M. Abdel-Hafez, S. Aswartham, A.U.B. Wolter, S. Wurmehl, C. Hess, K. Nenkov, G. Fuchs, D.V. Efremov, B. Holzapfel, J. van den Brink, and B. Büchner, Phys. Status Solidi B **250**, 593 (2013).
 - ³² SAINT+ (V. 2011), Bruker AXS Inc. (2011).
 - ³³ M. Sheldrick, SADABS (Version 2008/1), Bruker AXS Inc. (2008).
 - ³⁴ V. Petricek, M. Dusek, and L. Palatinus, JANA2006. The crystallographic computing system. Institute of Physics, Prague, Czech Republic (2006).
 - ³⁵ G. M. Sheldrick, Acta Crystallogr. Sect. A, **64**, 112 (2008).
 - ³⁶ P. L. Alireza and G. G. Lonczarich, Rev. Sci. Instrum. **80**, 023906 (2009).
 - ³⁷ N. Tateiwa, Y. Haga, T. D. Matsuda, and Z. Fisk, Rev. Sci. Instrum. **83**, 053906 (2012).
 - ³⁸ N. Tateiwa, Y. Haga, T. D. Matsuda, Z. Fisk, S. Ikeda and H. Kobayashi, Rev. Sci. Instrum. **84**, 046105 (2013).
 - ³⁹ Details about the pressure cell construction will be published elsewhere.
 - ⁴⁰ Institute of High-Pressure Physics, Polish Academy of Sciences, Unipress Equipment Division.
 - ⁴¹ L.D. Jennings and C.A. Swenson, Phys. Rev. **112**, 31 (1958).
 - ⁴² E. Gati, S. Köhler, D. Guterding, B. Wolf, S. Knöner, S. Ran, S.L. Bud'ko, P.C. Canfield, and M. Lang, Phys. Rev. B **86**, 220511(R) (2012).
 - ⁴³ J.K. Dong, S.Y. Zhou, T.Y. Guan, H. Zhang, Y.F. Dai, X. Qiu, X.F. Wang, Y. He, X.H. Chen, and S.Y. Li, Phys. Rev. Lett. **104**, 087005 (2010).
 - ⁴⁴ A.C. Jacko, J.O. Fjaerestad, B.J. Powell, Nature Phys. **5**, 422 (2009).
 - ⁴⁵ R.J. Radtke, K. Levin, H.B. Schuttler, M. R. Norman,

- Phys. Rev. B **48**, 653 (1993).
- ⁴⁶ P. Walmsley, C. Putzke, L. Malone, I. Guillamon, D. Vignolles, C. Proust, S. Badoux, A.I. Coldea, M.D. Watson, S. Kasahara, Y. Mizukami, T. Shibauchi, Y. Matsuda, and A. Carrington, Phys. Rev. Lett. **110**, 257002(2013).
- ⁴⁷ F. Rullier-Albenque, D. Colson, A. Forget, P. Thuery, and S. Poissonnet, Phys. Rev. B **81**, 224503 (2010).
- ⁴⁸ J. Engelmann, V. Grinenko, P. Chekhonin, W. Skrotzki, D.V. Efremov, S. Oswald, K. Iida, R. Hühne, J. Hänisch, M. Hoffmann, F. Kurth, L. Schultz, and B. Holzapfel, Nature Communications **4** (2013) 2877.
- ⁴⁹ S. Avci, O. Chmaissem, D.Y. Chung, S. Rosenkranz, E.A. Goremychkin, J.P. Castellán, I.S. Todorov, J.A. Schlueter, H. Claus, A. Daoud-Aladine, D.D. Khalyavin, M.G. Kanatzidis, and R. Osborn, Phys. Rev. B **85**, 184507 (2012).
- ⁵⁰ The uniaxial pressure derivatives were obtained using the Ehrenfest relation, i.e., in the limit of zero external pressure.^{17,20} In the case of Na substituted samples the effect of chemical pressure is rather strong (about 0.5 - 1.5 GPa). In such high pressures the ratio between pressure derivatives may be different from the estimated one using the Ehrenfest relation. However, taking into account that $T_c(P)$ of all (K,Na)-122 samples varies nearly linear up to 1.5 GPa and $T_{c0}(P)$ is independent on the Na substitution (see Section III.A), we concluded that the ratio between the pressure derivatives is nearly unchanged up to 1.5 GPa.
- ⁵¹ G. Kresse and J. Furthmüller, Phys. Rev. B **54**, 11169 (1996).
- ⁵² G. Kresse and J. Furthmüller, Comput. Mater. Sci. **6**, 15 (1996).
- ⁵³ G. Kresse and D. Joubert, Phys. Rev. B **59**, 1758 (1999).
- ⁵⁴ J.P. Perdew, K. Burke, and M. Ernzerhof, Phys. Rev. Lett. **77**, 3865 (1996).
- ⁵⁵ P.E. Blöchl, Phys. Rev. B **50**, 17953 (1994).
- ⁵⁶ H.J. Monkhorst and J.D. Pack, Phys. Rev. B **13**, 5188 (1976).
- ⁵⁷ V. Mishra, G. Boyd, S. Graser, T. Maier, P.J. Hirschfeld, and D.J. Scalapino, Phys. Rev. B **79**, 094512 (2009).
- ⁵⁸ Y. Wang, A. Kreisel, P.J. Hirschfeld, and V. Mishra, Phys. Rev. B **87**, 094504 (2013).
- ⁵⁹ P.M.C. Rourke, S.R. Julian, Comp. Phys. Comm. **183**, 324 (2012).
- ⁶⁰ T. Yoshida, S. Ideta, I. Nishi, A. Fujimori, M. Yi, R.G. Moore, S.K. Mo, D.-H. Lu, Z.-X. Shen, Z. Hussain, K. Kihou, P.M. Shirage, H. Kito, C.H. Lee, A. Iyo, H. Eisaki, and H. Harima, Front. Phys. **2**, 17 (2014).
- ⁶¹ T. Sato, K. Nakayama, Y. Sekiba, P. Richard, Y.-M. Xu, S. Souma, T. Takahashi, G.F. Chen, J.L. Luo, N.L. Wang, and H. Ding, Phys. Rev. Lett. **103**, 047002 (2009).
- ⁶² D.A. Zocco, K. Grube, F. Eilers, T. Wolf, H. v. Löhneysen, JPS Conf. Proc. **3**, 015007 (2014).
- ⁶³ T. Terashima, M. Kimata, N. Kurita, H. Satsukawa, A. Harada, K. Hazama, M. Imai, A. Sato, K. Kihou, C.-H. Lee, H. Kito, H. Eisaki, A. Iyo, T. Saito, H. Fukazawa, Y. Kohori, H. Harima, and S. Uji, Phys. Soc. Jpn. **79**, 053702 (2010).
- ⁶⁴ S. Backes, D. Guterding, H.O. Jeschke, R. Valenti, New J. Phys. **16**, 083025 (2014).
- ⁶⁵ Our DFT calculations did not show a Lifshitz transition under pressure up to 4 GPa for all experimentally observed Fermi surface sheets (α , ζ , β , and ϵ). We note that the small pillow at Z' point observed at $P = 0$ in the calculated band structure (see Fig. 6) disappears with the pressure. However, this particular Fermi surface sheet was not observed experimentally³, therefore in the analysis we ignored this pillow with a very small PDOS.